Understanding galaxy formation with ISO deep surveys [*]

David Elbaz
CEA Saclay/DSM/DAPNIA/Service d'Astrophysique
Orme des Merisiers, F-91191 Gif-sur-Yvette Cedex
France

Abstract. We present the results obtained through the various ISO extragalactic deep surveys. While IRAS revealed the existence of galaxies forming stars at a rate of a few tens (LIRGs) or even hundreds (ULIRGs) solar masses in the local universe, ISO not only discovered that these galaxies were already in place at redshift one, but also that they are not the extreme objects that we once believed them to be. Instead they appear to play a dominant role in shaping present-day galaxies as reflected by their role in the cosmic history of star formation and in producing the cosmic infrared background detected by the COBE satellite in the far infrared to sub-millimeter range.

1. General perspective

It is widely accepted that in the local universe stars form in giant molecular clouds (GMCs) where their optical and mostly UV light is strongly absorbed by the dust which surrounds them. Whether extinction was already taking place in the more distant universe where galaxies are less metal rich was less obvious ten years ago. Galaxies forming stars at a rate larger than about 20 $M_{\odot}$ yr^{-1} were known to radiate the bulk of their luminosity above 5 μm thanks to IRAS, the so-called luminous (LIRGs, $12 > log(L_{IR}/L_{\odot}) \geq 11$) and ultra-luminous (ULIRGs, $log(L_{IR}/L_{\odot}) \geq 12$) infrared (IR) galaxies. In the past, when galaxies were more gaseous and formed the bulk of their present-day stars, it would have been logical to expect to detect the past star formation events of galaxies in the IR regime and to detect a large population of LIRGs/ULIRGs too. However, prior to the launch of the Infrared Space Observatory (ISO, Kessler *et al.* 1996, Kessler *et al.* 2003), this idea was not widely spread. Partly because of a cultural reason: star formation rates (SFR) were commonly measured from optical emission lines and rest-frame UV light in galaxies. This may explain why the redshift evolution of the SFR density per unit comoving volume computed by Madau *et al.* (1996) became famous. However in the first presentation of the density of UV light

---

per unit comoving volume (Lilly *et al.* 1996) the authors were cautious to avoid converting their UV light into a SFR because of the unknown factor to correct for extinction. Already IRAS observations indicated a rapid decline of the comoving number density of ULIRGs since $z{\sim}0.3$ (Kim & Sanders 1998, see also Oliver *et al.* 1996), but this was over a small redshift range and with small number statistics. In the few years that followed the launch of ISO, several observations showed that galaxy formation could not be understood, at least on an observational basis, without accounting for dust extinction as a major ingredient. The ISO deep surveys played a major role in this process, together with other results summarized below. They clearly established that extreme events such as those taking place in local LIRGs and ULIRGs must have been more common in the past, so much that they can now be considered as a standard phase that most galaxies experienced during their lifetime, at least once, but maybe even several times.

The first result of the ISOCAM surveys, as well as the ISOPHOT ones, was the great difference of the counts measured at faint flux densities with respect to local ones from IRAS (Elbaz *et al.* 1999, Dole *et al.* 2001). The universe must have been much richer in IR luminous galaxies in the past, either because galaxies were more IR luminous, at fixed galaxy density, and/or because the number density of galaxies was larger in the past, which was partly expected due to the reverse effect of hierarchical galaxy formation through mergers. The strength of the excess of faint objects came as a surprise, but its consequences on the past star formation history of galaxies was confirmed by the convergence of other observations going in the same direction:

- the nearly simultaneous discovery of the cosmic infrared background (CIRB, Puget *et al.* 1996, Fixsen *et al.* 1998, Hauser & Dwek 2001 and references therein), at least as strong as the UV-optical-near IR one, whereas local galaxies only radiate about 30 % of their bolometric luminosity in the IR above $\lambda \sim 5\,\mu m$.

- the $850\,\mu m$ number counts from the SCUBA sub-millimeter bolometer array at the JCMT (Hughes *et al.* 1998, Barger *et al.* 1998, Smail *et al.* 2002, Chapman *et al.* 2003, and references therein) which also indicate a strong excess of faint objects in this wavelength range, implying that even at large redshifts dust emission must have been very large in at least the most active galaxies.

- the most distant galaxies, individually detected thanks to the photometric redshift technique using their Balmer or Lyman break signature showed the signature of a strong dust extinction. The so-called "β-slope" technique (Meurer *et al.* 1999) used to derive the intrinsic luminosity of these galaxies and correct their UV luminosity by factors of a few (typically between 3 and 7, Steidel *et al.* 1999, Adelberger & Steidel 2000) was later on shown to even underestimate the SFR of LIRGs/ULIRGs (Goldader *et al.* 2002).

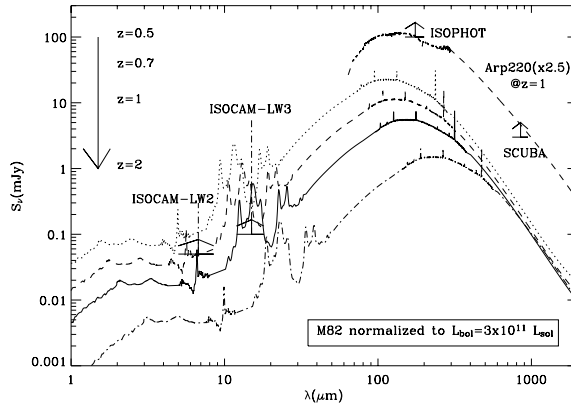- the slope of the sub-mJy deep radio surveys (Haarsma *et al.* 2000).

Figure 1. Effect of the k-correction on the detection of distant LIRGs and ULIRGs by ISO-CAM, ISOPHOT and SCUBA. Only ISOCAM at $15\,\mu$m can detect LIRGs up to $z \sim 1$, while ISOPHOT and SCUBA are sensitive to distant ULIRGs of a few 10^{12} L$_\odot$.

It has now become clear that the cosmic history of star formation based on rest-frame UV or emission line indicators of star formation such as [0II] or [Hα] strongly underestimate the true activity of galaxies in the past if not corrected by strong factors due to dust extinction. Although distant galaxies were less metal rich and much younger, they must have found the time to produce dust rapidly in order to efficiently absorb the UV light of their young stars.

We have tried to summarize in the following the role played by the ISO deep surveys in establishing this new perspective (see also Genzel & Cesarsky 2000). However, ten years after ISO's launch we are still trying to understand the consequences of these findings on galaxy formation scenarios. Are these distant LIRGs really similar to local ones ? What do they teach us about the connection between star and galaxy formation on one side (IMF, triggering of star formation, conditions of star formation,...) and between galaxy and large-scale structure formation on the other side (role of the environment in triggering star formation events, galaxy versus group and cluster formation, ellipticals versus spirals, ...) ? How much energy radiated by compton thick embedded active nuclei remains undetected even by the Chandra and XMM-Newton X-ray observatories ? These questions together with others that will be discussed in the following demonstrate the liveliness of this field that will continue to feed the next generation of telescopes and instruments to come such as Herschel, ALMA, the James Webb Space Telescope (JWST) or the Spitzer and GALEX space observatories presently in use.
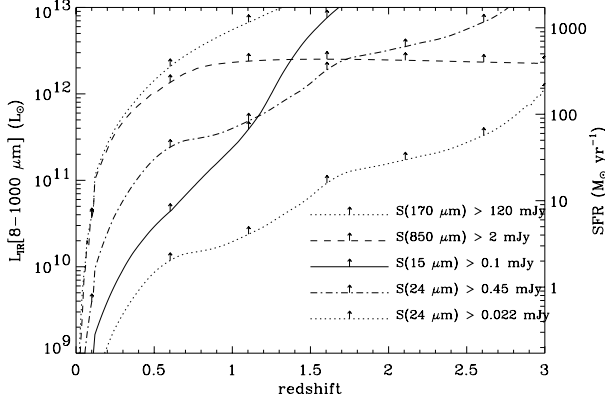
Figure 2. Sensitivity limits of ISOCAM ($15\,\mu$m, 0.1 mJy), ISOPHOT ($170\,\mu$m, 120 mJy), SCUBA ($850\,\mu$m, 2mJy) and Spitzer ($24\,\mu$m, 0.45 mJy and 0.022 mJy corresponding to the expected detection limits of the SWIRE and GOODS Legacy Programs). This figure was generated assuming that distant galaxies SEDs are similar to local ones. We used the library of template SEDs constructed by Chary & Elbaz (2001).

2. The ISO surveys

Extragalactic deep surveys with ISO were performed in the mid and far IR with ISOCAM (Cesarsky *et al.* 1996, Blommaert *et al.* 2003) and ISOPHOT (Lemke *et al.* 1996, Laureijs *et al.* 2003) respectively. In both wavelength ranges, the steep slopes of the number counts indicate that a rapid decline of the IR emission of galaxies must have taken place from around $z \sim 1$ to $z = 0$. As shown in Fig. 1, ISOCAM could detect galaxies at $15\,\mu$m in the LIRG regime up to $z \sim 1.3$, while ISOPHOT was limited to either nearby galaxies or moderately distant ULIRGs such as the one of $L_{IR} \sim 4 \times 10^{12}$ $L_\odot$ at a redshift of $z=1$ shown in the Fig. 1 (normalized SED of Arp 220). The detection limits of ISOCAM and ISOPHOT are compared to SCUBA and Spitzer in the Fig. 2. The deepest ISO surveys reached a completeness limit of 0.1 mJy at $15\,\mu$m (plain line) and a depth of $S_{15} \sim 40\,\mu$Jy (incomplete, Aussel *et al.* 1999) in blank fields or a twice deeper completeness level in the central part of nearby galaxy clusters using lensing magnification (Altieri *et al.* 1999, Metcalfe *et al.* 2003), and 120 mJy at $170\,\mu$m (dotted line). The right axis on the plot shows the conversion of the IR detection limit into a SFR detection limit. Any galaxy forming stars at a rate larger than 30 M$_\odot$ yr^{-1} could be detected with ISOCAM up to $z \sim 1$, assuming that the measured $15\,\mu$m flux density of a galaxy can be used to derive its "bolometric" IR luminosity, i.e. $L_{IR} = L(8\text{-}1000\,\mu$m$)$ (see Sect. 5.2).

Number counts represent the first scientific result of an extragalactic survey. They can be used to constrain the models. Used alone, they leave some

degeneracies unsolved but at least they can demonstrate whether the distant universe was different from the local one in this wavelength range by comparing them to "no evolution" predictions assuming some spectral energy distributions (SEDs) for the k-correction.

3. The ISOCAM 6.75 μm deep surveys

Deep images of blank fields at 6.75 and 15 μm done with ISOCAM provide a different view on the distant universe. While the ISOCAM-LW3 filter, centered at 15 μm, can probe dust emission up to $z \sim 2$ for luminous objects, the redshift range to probe star formation from dust emission with the ISOCAM-LW2 band, centered at 6.75 μm, is limited to the relatively nearby universe due to k-correction. However the emission of the old stellar component, which peaks in the near IR, being brought to this wavelength range for high-z galaxies, their stellar masses are better constrained from this flux density.

Sato *et al.* (2004) derived stellar masses around $M_\star \sim 10^{11}$ M$_\odot$ for galaxies with $z \sim 0.2$-3 from the correlation between rest-frame near IR luminosity and stellar mass. The stellar mass-to-light ratios were derived from model fit of the set of observed magnitudes depending on the galaxies star formation histories.

The contribution of the 6.75 μm selected galaxies to the cosmic stellar mass density of galaxies per unit comoving volume as a function of redshift were estimated to be comparable to those inferred from observations of UV bright galaxies (see Fig. 3). Given the narrow mass ranges, these estimates were obtained as simple summations of the detected sources and should therefore be considered as lower limits only. The faint 6.7 μm galaxies generally had red colors. A comparison with a particular population synthesis model suggests that they have experienced vigorous star formation at high redshifts. The derived large stellar masses for the faint 6.7 μm galaxies also support such star forming events at the past. However these events can only be detected at longer wavelengths using the 15 μm ISOCAM or 90 and 170 μm ISOPHOT bands with ISO (or SCUBA at 850 μm and now the Spitzer Space Telescope). The next sections are devoted to these surveys and their consequences on our understanding of the history of star formation in the universe.

4. The ISOPHOT far IR deep surveys

ISOPHOT was used to survey the sky at 90 and 170 μm, mainly (plus a few surveys at 60, 120, 150 and 180 μm, see Juvela *et al.* 2000; Linden-Voernle *et al.* 2000; cf review by Dole 2002). At 90 μm, the 46 arcseconds pixels and
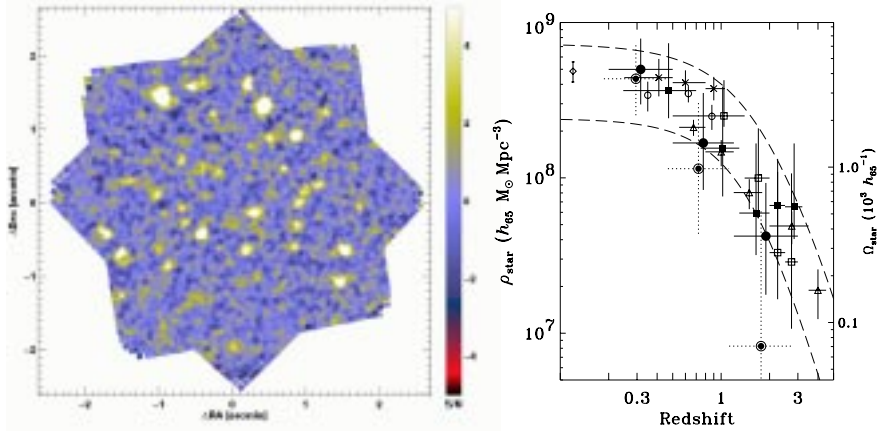
Figure 3. **(left)** ISOCAM 6.75 μm image of the SSA13 field (Fig.2 from Sato *et al.* 2003, 23 hour observation). This image reaches an 80 % completeness limit of 16 μJy in the central 7 arcmin^2 region. North is top and east to the left in J2000. The center is (RA, Dec) = ($13^h 12^m 26^s, 42°44' 24''.8$). The map shows signal-to-noise ratio (S/N) per 0.6 arcsec sub-pixel. The signal is an average, weighted by the inverse of the assigned variance, and the noise is a normalized standard deviation. **(right)** Stellar mass density in the universe as a function of redshift (Fig.13 from Sato *et al.* 2004). The right axis shows densities normalized to the critical density of the universe. The contributions of the 6.75 μm galaxies are shown with solid and double circles for the "combined" (including photometric redshifts) and purely spectroscopic samples, respectively. The double circles are plotted at slightly lower redshifts. The horizontal bars represent the redshift ranges of the bins and the vertical bars show one sigma errors, taking account of Poisson noise and uncertainties in stellar mass and V_{max}. Several other estimates are overlaid (see Sato *et al.* 2004 for references). The empty/solid squares and the diamond are obtained from full integration of a Schechter fit to their respective luminosity or stellar mass function at each redshift bin. The X marks and the empty circles are quasi-fully integrated values with a finite integration range from $10 L^*$ to $1/20 L^*$, and $10.5 < \log(M_{star} [h_{65}^{-2} M_\odot]) < 11.6$, respectively. The triangles are simply summed values of the detected sources. The two dashed curves are deduced by integrating the star formation rate density in the universe, which is derived from the UV luminosity density as a function of redshift (Cole *et al.* 2001). The upper curve is an extinction corrected case for $E(B-V) = 0.15$, and the lower one has no dust correction.

FWHM of ISOPHOT represented a significant improvement with respect to IRAS, however due to k-correction and sensitivity limitations, only the local universe could be probed at such wavelengths. The 170 μm band was more favorable for the detection of distant ULIRGs as shown in the Fig. 1 where the peak emission of a ULIRG of 4×10^{12} L$_\odot$ and redshifted at z=1 is shown (normalized SED of Arp 220). A major issue at these wavelengths with a 60 cm telescope is obviously the identification of optical counterparts for the determination of a redshift and the separation of local and distant galaxies.
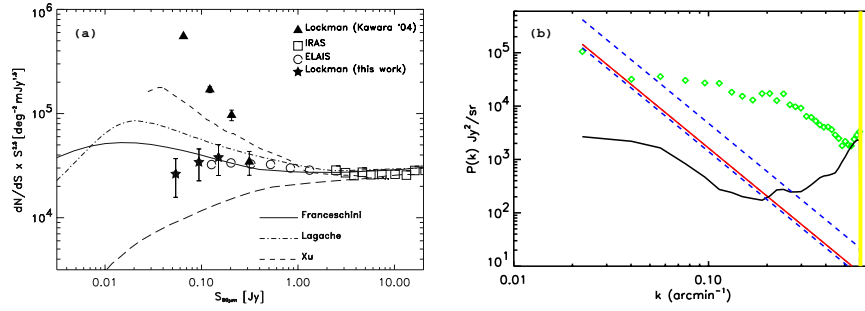
Figure 4. **(a)** Differential 90 μm counts dN/dS normalized to the Euclidean law ($N \propto S^{-2.5}$) (extracted from Rodighiero & Franceschini 2004). Results compared with those from the preliminary analysis of the ISOPHOT ELAIS survey (Efsthatiou *et al.* 2000, open circles) and with those from Kawara *et al.* (2004, filled triangles). The long-dashed line shows the expected contribution of non-evolving spirals as in the model of Franceschini *et al.* (2001). **(a)** Fluctuations of the CIB in a power spectrum analysis of the FIRBACK/ELAIS N2 field at 170 microns by Puget & Lagache (2000). Observed power spectrum: diamond; straight continuous line: the best fit cirrus power spectrum; dash line: cirrus power spectrum deduced from Miville-Deschênes *et al.* (2002); continuous curve: detector noise.

4.1. SOURCE COUNTS AND COSMIC IR BACKGROUND

Source counts at 170 μm (e.g. Kawara *et al.* , 1998; Puget *et al.* , 1999; Dole *et al.* , 2001) exhibit a steep slope of $\alpha = 3.3 \pm 0.6$ between 180 and 500 mJy and, like in the mid IR range, show sources in excess by a factor of 10 compared with no evolution scenario. The brightness fluctuations in the Lockman Hole were used by Matsuhara et al (2000) to constrain galaxy number counts down to 35 mJy at 90 μm and 60 mJy at 170 μm , confirming the existence of a strong evolution down to these flux densities. Using a new data reduction method, Rodighiero & Franceschini (2004) extended the previous works of Kawara *et al.* (1998), Efstathiou *et al.* (2000) and Linden-Voernle *et al.* (2000) down to lower flux densities (30 mJy at 90 μm) and found a clear excess of faint objects with respect to no evolution (see Fig. 4a). However, the resolved sources account for less than 10 % of the Cosmic Infrared Background at 170 μm , which is expected to be resolved into sources in the 1 to 10 mJy range.

   Sources below the detection limit of a survey create fluctuations. If the detection limit does not allow to resolve the sources dominating the CIB intensity, which is the case in the far IR with ISO, characterizing these fluctuations can constrain the spatial correlations of these unresolved sources of cosmological significance. An example of the modeled redshift distribution of the unresolved sources at 170 μm can be found in Fig. 12 of Lagache *et al.* (2003); the sources dominating the CIB fluctuations have a redshift distribution peaking at $z \sim 0.9$. After the pioneering work of Herbstmeierer

et al. (1998) with ISOPHOT, Lagache & Puget (2000) discovered them at 170 μm in the FIRBACK data, followed by other works at 170 and 90 μm (Matsuhara *et al.* 2000; Puget & Lagache, 2000; Kiss *et al.* 2001). Fig. 4b shows the CIB fluctuations in the FN2 field by Puget & Lagache, (2000), at wavenumbers $0.07 < k < 0.4$ arcmin^{-1}.

4.2. NATURE OF THE ISOPHOT GALAXIES

Determining the nature of the far IR galaxies has been a longer process than in the mid IR, mainly because of the difficulty to find the shorter wavelength counterparts in a large beam. Various techniques have been used to overcome this problem, one of the most successful being the identification using 20 cm radio data (e.g. Ciliegi *et al.* 1999). Another technique is the far IR multiwavelength approach (Juvela *et al.* 2000) that helps constraining the position and the SED; it also helps to separate the cirrus structures from the extragalactic sources. A variation is to use ISOCAM and ISOPHOT data, like the ELAIS Survey (Rowan-Robinson *et al.* 2004, see also Oliver in this book). Finally, the Serendipity Survey (Stickel *et al.* 1998, 2000), by covering large and shallow areas, allows to detect many bright objects easier to follow-up or already known.

Far IR ISO galaxies can be sorted schematically into two populations. First, the low redshift sources, typically $z < 0.3$ (e.g Serjeant *et al.* 2001; Patris *et al.* 2002, Kakazu *et al.* 2002), have moderate IR luminosities, below $10^{11}L_{\odot}$, and are cold (Stickel *et al.* 2000). Second, sources at higher redshift, $z \sim 0.3$ (Patris et al., 2002) and beyond, $z \sim 0.9$ (Chapman *et al.* 2002) are more luminous, typically $L > 10^{11}L_{\odot}$, and appear to be cold. Serjeant *et al.* (2001) derived the Luminosity Function at 90 μm, and started to detect an evolution compared to the local IRAS 100 μm sample.

5. The ISOCAM 15 μm deep surveys

A series of surveys were performed within the Garanteed Time (IGTES, ISO-CAM Garanteed Time Extragalactic Surveys, Elbaz *et al.* 1999) and Open Time as summarized in the Table I, where the surveys at 7 (6.75 μm) and 15 μm are sorted by increasing depth irrespective of wavelength. The major strength of ISOCAM is its spatial resolution (PSF FWHM of 4.5" at 15 μm, Okumura 1998) and sensitivity, which permitted to detect galaxies down to the LIRG regime up to $z \sim 1.3$ in the deepest surveys (Figs. 1, 2), well above confusion. Cosmic rays were a stronger limitation than photon or readout noise by inducing ghost sources when they were not perfectly removed, especially those with long term transients associated to them. Two techniques were developed in order to solve this issue, the so-called PRETI

Table I. *Table of the ISOCAM extragalactic surveys sorted by increasing depth. Col.(1) Survey name. Col. (2) wavelength of the survey with "7" for the LW2 filter centered at 6.75 μm and covering 5-8.5 μm, and "15" for the LW3 filter centered 15 μm and covering 12-18 μm. Col.(3) total area in square arcmin. Col.(4) integration time per sky position. Col.(5) depth (and 80% completeness limit when indicated). Col.(6) number of objects detected above this depth.*

Name	λ (μm)	Area ($'^2$)	Int.(min)	depth(mJy)	# objects
ELAIS N1[1]	15	9612	0.7;0.7	1;0.7	490
ELAIS N2[1]	7;15	9612;9612	0.7;0.7	1;0.7	628;566
ELAIS N3[1]	7;15	4752;3168	0.7;0.7	1;0.7	189;131
ELAIS S1[1]	7;15	6336;14256	0.7;0.7	1;0.7	304;317
ELAIS S2[1]	7;15	432;432	0.7;0.7	1;0.7	40;43
Lockman Shallow[2,3]	15	1944	3	0.25	457
		(80 % compl.)		0.45	260
Comet Field[4]	12	360	10	0.5	37
CFRS14+52[5]	7;15	100;100	18;11	0.3 ;0.4	23;41
CFRS03+00[6]	7;15	100;100	6;22	0.5 ;0.3	-
Lockman Deep[2,7]	7;15	500;500	18;11	0.3 ;0.4	166
Marano DSF[2]	7;15	900;900	15.4;15.4	0.19 ;0.32	180
A370[8]	7;15	31.3;31.3	42;42	0.052;0.21$^{(u)}$	4;20
		(80 % compl.)		0.080;0.293$^{(u)}$	
Marano UDSR[2]	7;15	85;90	120;114	0.18 ;0.14	-;142
Marano UDSF[2]	7;15	89;90	114	0.08 ;0.14	115;137
A2218[8]	7;15	20.5;20.5	84;84	0.054;0.121$^{(u)}$	18;46
		(80 % compl.)		0.079;0.167$^{(u)}$	
HDFN+FF[2,9]	7;15	10;27	116;135	0.05 ;0.1	7;44
HDFS[2,10]	7;15	28;28	168;168	0.05 ;0.1	16;63
A2390[11,8]	7;15	5.3;5.3	432;432	0.038;0.050$^{(u)}$	10;28
		(80 % compl.)		0.052;0.092$^{(u)}$	
Lockman PGPQ[12]	7	9	744	0.034	15
SSA13[13]	7	16	1264	0.006	65
		7(80 % compl.)		0.016	

References: (1) Oliver *et al.* 2000, Rowan-Robinson *et al.* 2004, (2) Elbaz *et al.* 1999 and in prep., (3) Rodighiero *et al.* 2004, (4) Clements et al. 1999, (5) Flores *et al.* 1999, (6) Flores (private communication), (7) Fadda *et al.* 2004, (8) Metcalfe *et al.* 2003, (9) Aussel *et al.* 1999, Goldschmidt *et al.* 1997, (10) Oliver *et al.* 2002, (11) Altieri *et al.* 1999, (12) Taniguchi et al. 1997, (13) Sato *et al.* 2003, Sato *et al.* 2004. The depth of the deep surveys in the field of lensing clusters does not include the correction for lensing amplification, as indicated by the $^{(u)}$
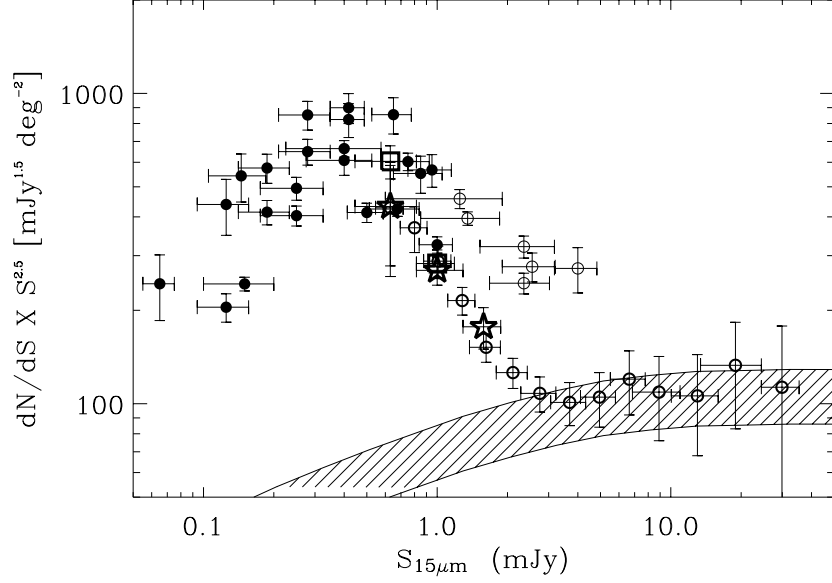
Figure 5. ISOCAM 15 μm differential counts, with 68% error bars. The counts are normalized to a Euclidean distribution of non-evolving sources, which would have a slope of $\alpha = -2.5$ in such a universe. This plot is an extension of the Fig.2 from Elbaz *et al.* (1999) combining the data points from Elbaz *et al.* (1999), for the ISOCAM Garanteed Time Extragalactic Surveys (IGTES, filled and empty dots for sources below and above 1 mJy respectively, see text), Gruppioni *et al.* (2003, bold empty circles) for the ELAIS-S1 field, Rodighiero *et al.* (2004, large open stars) and Fadda *et al.* (2004, large open squares), for the Shallow and Deep Surveys of the Lockman Hole respectively (analysis of the IGTES data using the "Lari" technique, see Sect. 5). The hatched area materializes the range of possible expectations from models assuming no evolution and normalized to the 15 μm local luminosity function (LLF) from Fang *et al.* (1998) and the template SED of M51 (with an assumed uncertainty of $\pm$ 20 %; this 15 μm LLF was recently confirmed over a larger sample of local galaxies by H.Aussel, private communication).

(Pattern REcognition Technique for Isocam data, Starck *et al.* 1999) and LARI (Lari *et al.* 2001) techniques. A third technique was developed by Désert *et al.* (1999), in which the mosaic data were analyzed using the beam switching approach, the Three Beam technique. PRETI consists in a multi-scale wavelet decomposition of the signal, while LARI tries to account for the physical processes taking place in the detectors, including the effect of neighboring pixels. The LARI technique was first applied to the ELAIS surveys (see Oliver *et al.* , in these book) and more recently to the IGTES surveys of the Lockman Hole (Rodighiero *et al.* 2004, Fadda *et al.* 2004) and of the Marano field (Elbaz *et al.* , in prep.). The quality of the ISOCAM images is shown with the case of the Marano FIRBACK deep field (30'$\times$30') in the
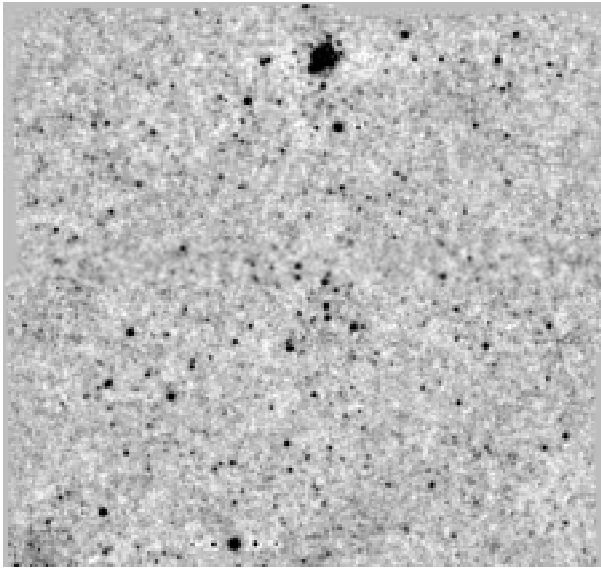
Figure 6. ISOCAM 15 μm image of the Marano FIRBACK Deep Survey (DSF) from the IGTES (Elbaz *et al.* 1999, and in prep.). Data reduction with PRETI.
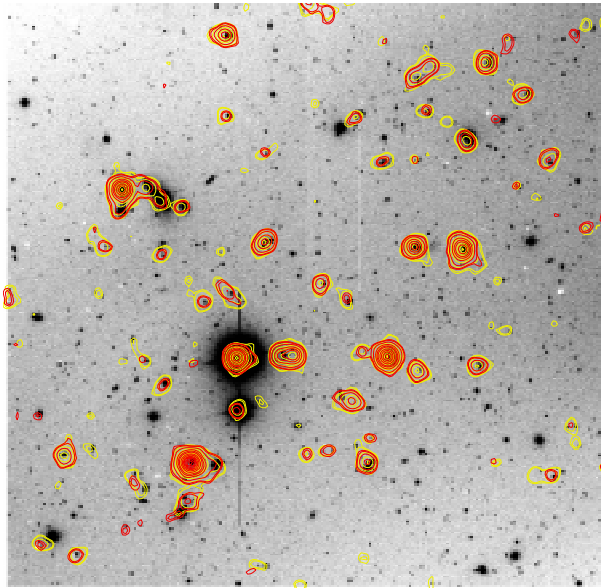

Figure 7. ISOCAM 15 μm contours overlayed on the VLT-FORS2 image (7' ×7', R-band) of the Marano FIRBACK Ultra Deep Survey (UDSF). The LARI (light contours, yellow on screen, grey on paper) and PRETI (dark contours, red on screen) detect the same objects.
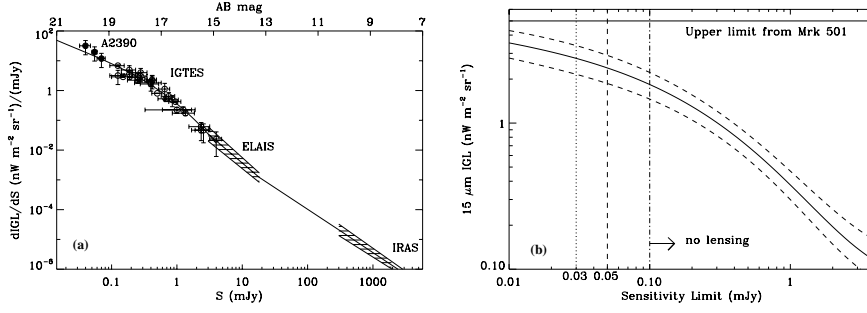
Figure 8. **a)** Differential contribution to the 15 μm Integrated Galaxy Light as a function of flux density and AB magnitude. The plain line is a fit to the data: Abell 2390 (Altieri *et al.* 1999), the ISOCAM Guaranteed Time Extragalactic Surveys (IGTES, Elbaz *et al.* 1999), the European Large Area Infrared Survey (ELAIS, Serjeant *et al.* 2000) and the IRAS all sky survey (Rush, Malkan & Spinoglio 1993). **b)** Contribution of ISOCAM galaxies to the 15 μm extragalactic background light (EBL), i.e. 15 μm Integrated Galaxy Light (IGL), as a function of sensitivity or *AB* magnitude $\left(AB = -2.5\,log\left(S_{\mathrm{mJy}}\right)+16.4\right)$. The plain line is the integral of the fit to dIGL/dS (Fig.a). The dashed lines correspond to 1-σ error bars obtained by fitting the 1-σ upper and lower limits of dIGL/dS.

Fig. 6. The central part of this field was imaged at a deeper level (UDSF) and analyzed with both techniques. The resulting contours are overlayed on a VLT-FORS2 image of the field, demonstrating the consistency and robustness of both source detection algorithms (Fig. 7).

Lensing appeared to be a very powerful tool to extend the detection of faint objects by a factor 2-3 (see Metcalfe *et al.* 2003). However studies such as the relative clustering of IR galaxies versus field galaxies are better done in larger homogeneous fields, where the role of cosmic variance can also be quantified. As we will see below, the environment of distant LIRGs seems to play a major role in triggering their star formation activity.

5.1. Source Counts and Cosmic IR Background

The source counts at 15 μm exhibit a strong excess of faint sources below $S_{15} \sim 2$ mJy. This excess is usually defined by comparison with model predictions assuming that galaxies behaved similarly in the distant universe as they do today. Such "no evolution" behavior is represented by a shaded area in the Fig. 5 (see figure caption). Galaxies above this flux density do fall within this region, as illustrated by the data points from the ELAIS-S1 field (Gruppioni *et al.* 2003, see also Oliver *et al.* in this book). In Fig. 5, we have separated the data points from the IGTES (Elbaz *et al.* 1999) between those below and above $S_{15} = 1$ mJy, with filled and open dots respectively. Data above this flux density from Elbaz *et al.* (1999) appear to be inconsistent with those derived from ELAIS-S1. Most of those points were derived from

the Shallow Survey of the Lockman Hole within the IGTES, which suffered from having less redundant observations of a given sky pixel. At that time, ISOCAM data reduction methods were not optimized for such surveys, but since then, they have been improved to better deal with such shallow surveys. Among the techniques that are discussed below, the "Lari" technique is particularly suitable for such low redundancy surveys (and even more for the very shallow ELAIS surveys, see Oliver *et al.* in this book) and a recent analysis of the Lockman Hole Deep (Fadda *et al.* 2004, large open squares) and Shallow (Rodighiero *et al.* 2004, large open stars) surveys from the IGTES provided new number counts at these flux densities perfectly consistent with those derived from ELAIS-S1 by Gruppioni *et al.* (2003) also using the same "Lari" technique. Note that the models designed to fit the ISOCAM number counts were constrained by the Elbaz *et al.* (1999) results, hence overproduce the number of sources above $S_{15} \sim 2$ mJy. As a natural result, they have also overpredicted the number of sources detected in the high flux density regime at $24\,\mu$m with Spitzer (see Sect. 7 and Papovich *et al.* 2004, Chary *et al.* 2004).

Above the Earth's atmosphere, the $15\,\mu$m light is strongly dominated by the zodiacal emission from interplanetary dust and it has not yet been possible to make a direct measurement of the $15\,\mu$m background, or EBL. Individual galaxies contribute to this background and a lower limit to the $15\,\mu$m EBL can be obtained by adding up the fluxes of all ISOCAM galaxies detected per unit area down to a given flux limit. The resulting value is called the $15\,\mu$m integrated galaxy light (IGL).

As in Elbaz *et al.* (2002), the differential number counts can be converted into a differential contribution to the $15\,\mu$m IGL as a function of flux density, estimated from the following formula:

$$\frac{dIGL}{dS} = \frac{dN}{dS} \times \left(\frac{S_{15}}{10^{20}}\right) \times \nu_{15} \qquad (1)$$

where $dN(\mathrm{sr}^{-1})$ is the surface density of sources with a flux density $S_\nu[15\,\mu\mathrm{m}]= S_{15}$ (mJy) over a flux density bin dS(mJy) (1 mJy= 10^{-20} nW m^{-2} Hz^{-1}) and ν_{15}(Hz) is the frequency of the $15\,\mu$m photons.

About 600 galaxies below $S_{15} \sim 3$ mJy, were used to provide the points with errors bars in Fig. 8a. Fig. 8b shows the $15\,\mu$m IGL as a function of depth. It corresponds to the integral of Fig. 8a, where the data below 3 mJy were fitted with a polynomial of degree 3 and the 1-σ error bars on $dIGL/dS$ were obtained from the polynomial fit to the upper and lower limits of the data points. The $15\,\mu$m IGL does not converge above a sensitivity limit of $S_{15} \sim 50\,\mu$Jy, but the flattening of the curve below $S_{15} \sim 0.4$ mJy suggests that most of the $15\,\mu$m EBL should arise from the galaxies already unveiled by ISOCAM. Above this flux density limit, where the completeness limit is larger than 80 % - including lensed objects-, it is equal to 2.4 $\pm$ 0.5 nW m^{-2} sr^{-1} (Elbaz *et al.* 2002). Down to a 50 % completeness limit, Metcalfe

et al. (2003) found a 10 % larger value including sources down to $30\,\mu$Jy but the statistics remains limited at these depths with only four sources below $50\,\mu$Jy.

Franceschini et al. (2001) and Chary & Elbaz (2001), developed models which reproduce the number counts from ISOCAM at $15\,\mu$m, from ISOPHOT at 90 and $170\,\mu$m and from SCUBA at $850\,\mu$m, as well as the shape of the CIRB from 100 to $1000\,\mu$m. These models consistently predict a $15\,\mu$m EBL of:

$$EBL^{models}(15\,\mu\text{m}) \sim 3.3 \text{ nW m}^{-2}\text{ sr}^{-1} \tag{2}$$

If this prediction from the models is correct then about 73 ± 15 % of the $15\,\mu$m EBL is resolved into individual galaxies by the ISOCAM surveys.

This result is consistent with the upper limit on the $15\,\mu$m EBL estimated by Stanev & Franceschini (1998) of:

$$EBL^{max}(15\,\mu\text{m}) \sim 5 \text{ nW m}^{-2}\text{ sr}^{-1} \tag{3}$$

This upper limit was computed from the 1997 γ-ray outburst of the blazar Mkn 501 ($z = 0.034$) as a result of the opacity of mid IR photons to γ-ray photons, which annihilate with them through e^+e^- pair production. It was since confirmed by Renault et al. (2001), who found an upper limit of 4.7 nW m^{-2} sr^{-1} from 5 to $15\,\mu$m.

Nearly all the IGL is produced by sources fainter than 3 mJy (94 %) and about 70 % by sources fainter than 0.5 mJy. This means that the nature and redshift distribution of the galaxies producing the bulk of the $15\,\mu$m IGL can be determined by studying these faint galaxies only.

5.2. MID IR AS A SFR INDICATOR

When normalized to the $7.7\,\mu$m PAH (polycyclic aromatic hydrocarbon) broad emission line, the spectra of different galaxies exhibit very different 15, 25, 60 or $100\,\mu$m over $7.7\,\mu$m ratio. This was often interpreted as an indication that measuring the monochromatic luminosity of a galaxy at one mid IR wavelength was useless to determine its bolometric IR luminosity, $L_{IR} = L(8$–$1000\,\mu$m). However, the variation of the far over mid IR ratio is correlated with L_{IR} and local galaxies do exhibit a strong correlation of their mid and far IR luminosities (Fig. 9). These correlations can be used to construct a family of template SEDs or correlations from which the L_{IR} , and therefore SFR, of a galaxy can be derived from its mid IR luminosity (Chary & Elbaz 2001, Elbaz *et al.* 2002). The L_{IR} derived from this technique are consistent with those derived by the radio-far IR correlation, when radio-mid-far IR data exist (Elbaz *et al.* 2002, Garrett 2002, Gruppioni *et al.* 2003). In the Fig. 10, we have reproduced the plot from Elbaz *et al.* (2002) complemented with galaxies detected within the ELAIS survey (Rowan-Robinson *et al.* 2004).
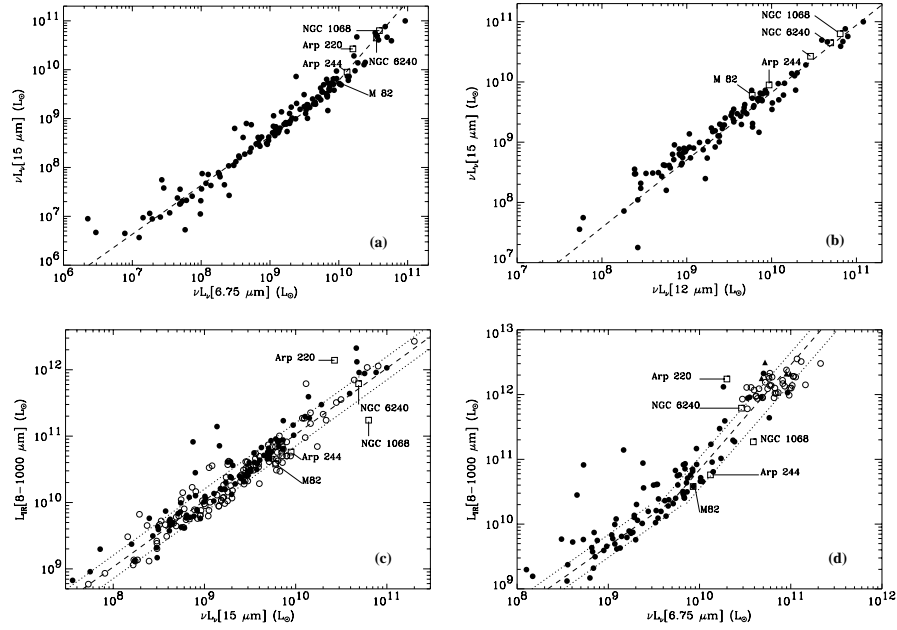
Figure 9. IR luminosity correlations for local galaxies (from Elbaz *et al.* 2002). **a)** ISO-CAM-LW3 (15 μm) versus ISOCAM-LW2 (6.75 μm) luminosities (νL_ν) (56 galaxies). **b)** ISO-CAM-LW3 (15 μm) versus IRAS-12 μm luminosities (45 galaxies). **c)** L_{IR}[8-1000 μm] versus ISOCAM-LW3 (15 μm) luminosity (120 galaxies). **d)** L_{IR}[8-1000 μm] versus LW2-6.75 μm luminosities (91 galaxies). Filled dots: galaxies from the ISOCAM guaranteed time (47 galaxies including the open squares). Open dots: 40 galaxies from Rigopoulou *et al.* (1999). Empty triangles: 4 galaxies from Tran et al. (2001). Galaxies below $L_{IR} \sim 10^{10}$ L$_\odot$ present a flatter slope and have $L_{IR}/L_B < 1$.

Except at low luminosities were the contribution of cirrus to the IR luminosity becomes non negligible, the 1.4 GHz and 15 μm rest-frame luminosities are correlated up to $z \sim 1$ and therefore predict very consistent total IR luminosities. A similar result was later on obtained using the MIPS instrument onboard the Spitzer Space Observatory at 24 μm (Appleton *et al.* 2004).

Several studies compared the SFR derived from the IR luminosity with the optical SFR derived from the Hα emission line (Rigopoulou *et al.* 2000, Cardiel *et al.* 2003, Flores *et al.* 2004, Liang *et al.* 2004). Rigopoulou *et al.* (2000) found a large excess of SFR(IR) versus SFR(Hα) even after correcting the latter for extinction. The Balmer decrement was only measured for limited number of objects in the sample and the extinction correction was derived from broadband photometry, which suffers from strong uncertainties in particular due to the degeneracy between age, metallicity and extinction. However, Cardiel *et al.* (2003) confirmed the direct measure of the SFR(IR) excess using the combination of NIRSPEC and LRIS, for the distant galaxies, and
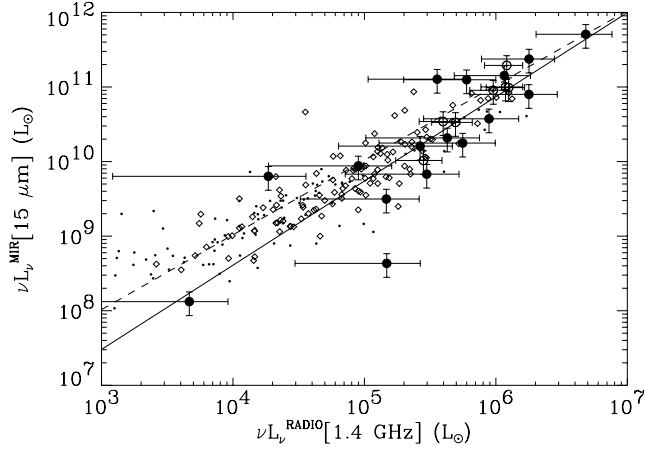
Figure 10. 15 μm versus radio continuum (1.4 GHz) rest-frame luminosities. Small filled dots: sample of 109 local galaxies from ISOCAM and NVSS. Filled dots with error bars: 17 HDFN galaxies ($z \sim$0.7, radio from VLA or WSRT). Open dots with error bars: 7 CFRS-14 galaxies ($z \sim$0.7, Flores *et al.* 1999, radio from VLA). Open diamonds: 137 ELAIS galaxies ($z \sim$ 0-0.4).

the Echelle Spectrograph and Imager (ESI), for the closer ones, at the Keck telescope. Using high resolution VLT-FORS2 spectra, Flores *et al.* (2004) and Liang *et al.* (2004) were able to measure directly the Balmer decrement (using Hα/Hβ or Hβ/Hγ) and to subtract the underlying nebular emission lines with a fit of the stellar continuum. Although the SFR(IR) exceeds the estimate from emission lines for the most active objects, the data present a clear correlation between SFR(IR) and SFR(Hα) which suggests that the star formation regions responsible for the IR luminosity of distant LIRGs are not completely obscured. This correlations also confirms that the mid IR is indeed a good SFR estimator.

5.3. NATURE OF THE ISOCAM GALAXIES

The Hubble Deep Field North and its Flanking Fields (HDFN+FF) provides the best coverage in spectroscopic redshifts and deep optical images for an ISOCAM deep survey. We used the revised version of the Aussel *et al.* (1999) catalog for which 85 % (71 %) of the 40 (86) galaxies above $100\,\mu$Jy ($30\,\mu$Jy) have a spectroscopic redshift to determine the average properties of ISOCAM galaxies summarized in the Figs. 11, 12. Their optical counterparts are relatively bright and their median-mean redshift is close to $z \sim$0.8 (Fig. 11). Note the redshift peaks in which the ISOCAM galaxies are located, leaving wide empty spaces in between. Most ISOCAM galaxies are located within large-scale structures, here mainly those at z=0.848 and z=1.017, which might be

galaxy clusters in formation where galaxy-galaxy interactions are amplified (Elbaz & Cesarsky 2003, see discussion below).

Thanks to the deepest soft to hard X-ray survey ever performed with Chandra in the HDFN, it is possible to pinpoint active galactic nuclei (AGNs) in this field including those affected by dust extinction. Only five sources were classified as AGN dominated on the basis of their X-ray properties (Fadda et al. 2002). Hence, unless a large number of AGNs are so dust obscured that they were even missed with the 2 Megaseconds Chandra survey, the vast majority of ISOCAM galaxies are powered by star formation. This result is consistent with observations of local galaxies which indicate that only the upper luminosity range of ULIRGs are dominated by an AGN (Tran *et al.* 2001).

Using the mid-far IR correlations (Chary & Elbaz 2001, Elbaz *et al.* 2002, see also Sec. 5.2), the L_{IR} distribution of the HDFN mid IR sources is plotted in Fig. 12a. Most of them belong to the LIRG and ULIRG regime, although when including flux densities below completeness down to $30\,\mu$Jy, one finds also intermediate luminosities. Finally, their stellar masses are among the largest in their redshift range, when compared to the stellar mass estimates by Dickinson *et al.* (2003) in the HDFN (Fig. 12b).

In the local universe, both LIRGs and ULIRGs exhibit the typical morphology of major mergers, i.e. mergers of approximately equal mass (Sanders & Mirabel 1996, Sanders, Surace & Ishida 1999). In the case of LIRGs, the merging galaxies show a larger separation than for ULIRGs, which are mostly in the late phase of the merger. Fig. 13 (Elbaz & Moy 2004) presents the HST-ACS morphology of a sample of $z \sim 0.7$ LIRGs in the GOODSN field (extended HDFN). Less than half of these galaxies clone the morphology of local LIRGs, which implies that the physical processes switching on the star formation activity in distant LIRGs might be different than for local ones. The gas mass fraction of younger galaxies being larger, other types of interactions might generate a LIRG phase in the distant universe, such as minor mergers or even passing-by galaxies producing a tidal effect. The fact that such interactions are more frequent than major mergers could also explain the importance of the LIRG phase for galaxies in general and also the possibility for a galaxy to experience several intense bursts in its lifetime. The appearance of this phase of violent star formation could be facilitated during the formation of groups or clusters of galaxies.

A striking example of this is given by the large fraction of LIRGs detected in the distant galaxy cluster J1888.16CL, located at a redshit of $z = 0.56$ (Duc *et al.* 2004). Among the 27 objects for which spectra were obtained, six of them belong to the cluster while an extra pair with slightly higher redshifts may lie in infalling groups. All eight galaxies exhibit weak emission lines in their optical spectra, typical of dust enshrouded star forming galaxies, none of these lines being broad enough to indicate the presence of type I AGNs.

In this relatively young galaxy cluster, the mechanism that may be triggering SFRs between 20 and 120 M⊙ yr^{-1} for at least eight objects of the cluster could well be tidal collisions within sub-structures or infalling groups. On a more local scale, the mid IR emission of the Abell 1689 ($z = 0.181$) galaxies exhibits an excess of the B-[15] color with respect to richer and closer galaxy clusters, such as Coma and Virgo, which suggests the presence of a mid IR equivalent to the Butcher-Oemler effect, i.e. the star formation activity of galaxies as reflected by their mid IR emission increases with increasing red-shift (Fadda *et al.* 2000). The high fraction of blue galaxies intially reported for this cluster by Butcher & Oemler (1984) was later on confirmed by Duc *et al.* (2002), who also found that the actual SFR for these galaxies was on average ten times larger than the one derived from the [OII] emission line implying that 90 % of the star formation activity taking place in this cluster was hidden by dust.

LIRGs could then be a tracer of large-scale structures in formation as suggested by their redshift distribution (Fig. 11b, see also Elbaz & Cesarsky 2003). In order to test this hypothesis, Moy & Elbaz (in prep.) compared the fraction of ISOCAM galaxies (above the completeness limit of 0.1 mJy) found in "redshift peaks" to the one obtained when randomly selecting field sources of equal optical and K-band magnitudes in the same redshift range. Redshift peaks of different strengths, measured as N-σ, were defined by smooth-ing the field galaxies redshift distribution by 15,000 km/s (Fig.14a) and mea-suring the peaks N-σ above the smoothed distribution. The Monte-Carlo sam-ples of field galaxies to be compared to the redshift distribution of the ISO-CAM galaxies were selected within the real redshift distribution and not the smoothed one. The distribution of the Monte-Carlo simulations are shown with error bars at the 68 and 90 % level. When considering the whole ISO-CAM catalog, i.e. including faint sources below completeness, it appears that ISOCAM galaxies are more clustered than field galaxies. Less than 32 % of the simulations present a comparable clustering than the whole ISOCAM sample which contains a large fraction of non LIRGs. Strickingly, when only selecting the brightest galaxies above the completeness limit of 0.1 mJy, one finds that they are LIRGs and ULIRGs which fall in the densest redshift peaks, above 6-σ. The probability to randomly select a sample of galaxies from the field (with equal magnitudes and redshift range) in the redshift peaks of 6-σ and above is less than 1 %. As a result, mid IR surveys are very efficient in selecting over-dense regions in the universe, which in return are very efficient in producing a LIRG. On the contrary, mid IR selected galaxies are locally less clustered than field galaxies (Gonzalez-Solares *et al.* 2004), which could be a natural result of the fact that only the less clustered galaxies still produce IR luminous phases while more clustered galaxies lived their IR luminous phase in the past (see also Elbaz & Cesarsky 2003).
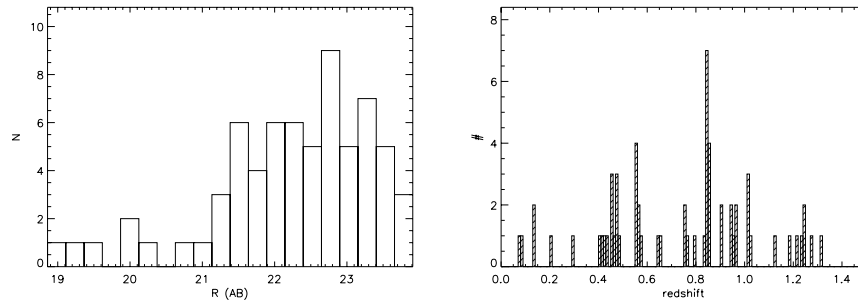
Figure 11. (left) Histogram of the R(AB) magnitudes of the $15 \, \mu m$ ISOCAM galaxies detected in the HDFN+FF (revised catalog of Aussel *et al.* down to $\sim 30 \, \mu$Jy. (right) Redshift distribution of the HDFN+FF ISOCAM galaxies.

Finally, one question remains to be addressed about distant LIRGs: how long does this starburst phase last and how much stellar mass is produced during that time ? Marcillac *et al.* (2004) used a bayesian approach and simulated 200,000 virtual high-resolution spectra with the Bruzual & Charlot (2003) code to determine the recent star formation history of distant LIRGs as well as their stellar masses. These ISOCAM galaxies were observed using the VLT-FORS2 ($\Delta\lambda/\lambda \sim 2000$ in the rest-frame) in three different fields. A prototypical LIRG at $z \sim 0.7$ is found to have a stellar mass of $\sim 5 \times 10^{10}$ $M_\odot$ and to produce about 10 % of this stellar mass within about 10^8 years during the burst. A remarkable result of this study is that the position of distant LIRGs in a diagram showing the value of the H8 Balmer absorption line equivalent width versus the strength of the 4000 Å break signs the presence of a burst of star formation within these galaxies, with an intensity of about $50 \, M_\odot \, \text{yr}^{-1}$ as also derived from their mid IR emission. This result supports the idea that distant LIRGs are not completely opaque to optical light and that one can learn something about their star formation history based on their optical spectra.

Liang *et al.* (2004) compared the gas metallicity of the same sample of objects than Marcillac *et al.* (2004) with local galaxies of similar absolute magnitudes in the B band. Even accounting for an evolution in the B-band luminosity, the distant LIRGs turn out to be about twice less metal rich. This result suggests that between $z \sim 1$ and today, LIRGs do produce a large fraction of the metals located in their host galaxies in agreement with the strong evolution of the cosmic star formation history found by the models fitting the ISO source counts.
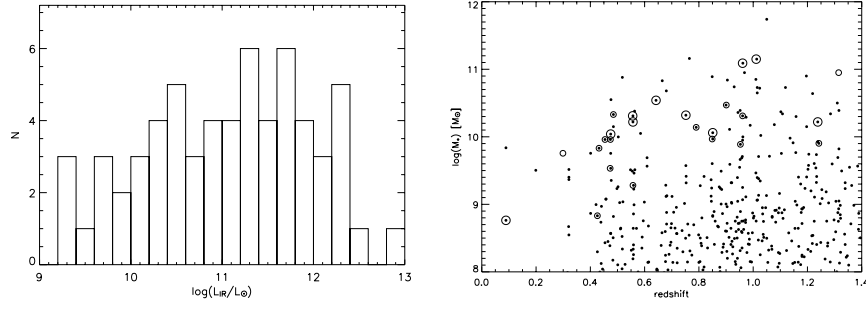
Figure 12. (left) Distribution of the log(L_{IR} (8-1000 μm)/$L_\odot$) of the HDFN+FF ISOCAM galaxies derived from ther 15 μm flux densities. (right) Stellar mass as a function of redshift of field HDFN proper galaxies (dark dots) and of ISOCAM galaxies (open circles). All stellar masses were derived using multi-bands SED modelling by Dickinson *et al.* (2003).
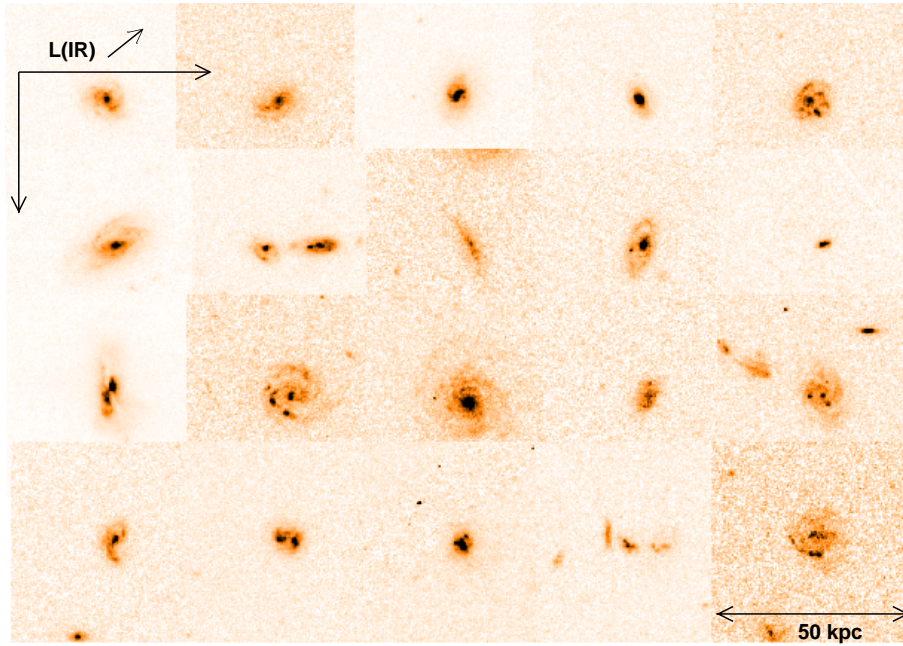

Figure 13. HST-ACS images of LIR galaxies with $11 \leq \log(L_{IR}/L_\odot) \leq 12$ (LIRGs) and $z \sim 0.7$. The double-headed arrow indicates the physical size of 50 kpc. The IR luminosity increases from left to right and from top to bottom.

6. Cosmic evolution, star formation rate history

The combination of surveys at different wavelengths, from ISOCAM, ISOPHOT and SCUBA, together with the the shape and intensity of the CIRB, was used by several authors to constrain the parameters of their backward evolution models assuming a combination of luminosity and density evolution as a
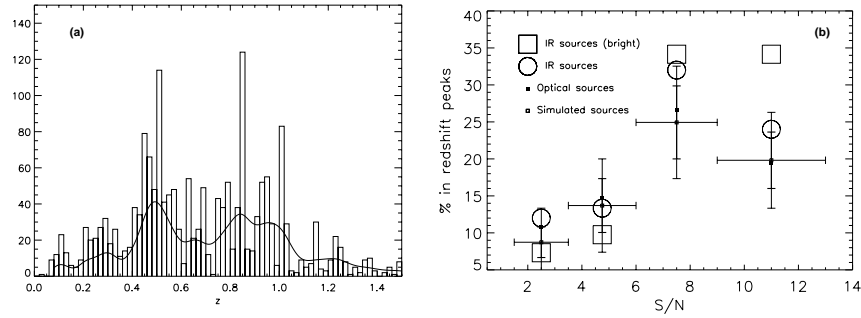
Figure 14. **(a)** Redshift distribution of field galaxies in the GOODSN field. The continuous line is the smoothed distribution with a window of 15,000 km/s. **(b)** Differential fraction of sources within redshift peaks (see definition in the text) stronger than N-σ. Small filled squares: fraction of sources in peaks for the whole optical catalog of 930 field galaxies (Wirth *et al.* 2004). Small open squares: median of the fraction of sources in redshift peaks for a series of Monte Carlo simulations of a sub-sample of the field galaxies corresponding to the same number of galaxies as in the ISOCAM catalog and within the same range of redshifts and optical-near IR magnitudes. Error bars contain 68 and 90 % of the simulations. Large Open Circles: total sample of ISOCAM galaxies (75 sources with spectroscopic redshifts and optical-near IR magnitudes). Large open squares: sub-sample of ISOCAM galaxies above the completeness limit of 0.1 mJy (41 sources).

function of redshift of the IR luminosity function at 15 or $60\,\mu$m: Roche & Eales (1999), Tan *et al.* (1999), Devriendt & Guiderdoni (2000), Dole *et al.* (2000), Chary & Elbaz (2001), Franceschini *et al.* (2001, 2003), Malkan & Stecker (2001), Pearson (2001), Rowan-Robinson (2001), King & Rowan-Robinson (2003), Takeuchi *et al.* (2001), Xu *et al.* (2001,2003), Balland *et al.* (2002), Lagache, Dole & Puget (2003), Totani & Takeuchi (2002), Wang (2002).

Being limited by the sensitivity of the extragalactic surveys, the major output of these models was to show that LIRGs and ULIRGs were much more common in the past than they are today. Chary & Elbaz (2001) derived that the comoving IR luminosity due to LIRGs was about seventy times larger at $z \sim 1$ than it is today (Fig. 15). Quite logically, it resulted that the contribution of LIRGs to the cosmic star formation history was so large in the past that it dominated the integrated star formation that galaxies experienced in the past. Hence, LIRGs should now be considered not as a type of galaxies but instead as a common phase of intense star formation that any galaxy may have experienced.

Elbaz *et al.* (2002) derived the contribution to the peak of the CIRB at $140\,\mu$m from the population of LIRGs around $z \sim 0.8$ detected in the ISO-CAM $15\,\mu$m deep surveys and found that these objects alone can explain more than two thirds of the peak and integrated intensities of the CIRB (see Fig. 16). Hence the CIRB is the signature of the strong redshift evolution of
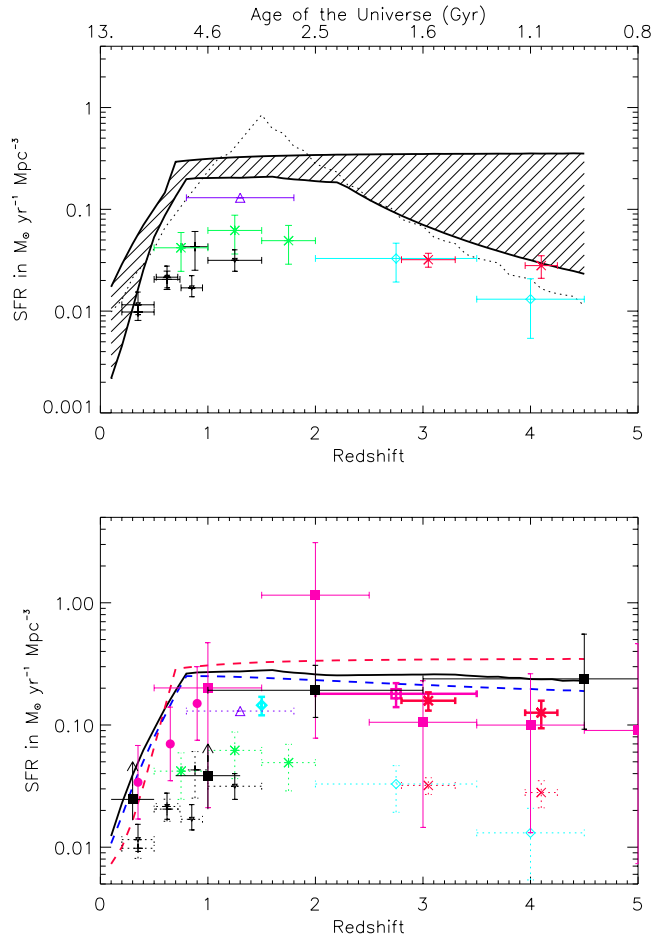
Figure 15. Star Formation Rate from Chary & Elbaz (2001). Upper panel: min and max range from their model, and observed UV/opt data; dots represent Xu *et al.* (2001) model. Lower panel: 3 different evolution scenarios from their model and data corrected for extinction. Line: pure luminosity; upper dash: pure density; lower dash: luminosity+density.

LIRGs and the fossil record of star formation which took place in such burst phases.

7. From ISO to Spitzer, Herschel, the JWST and ALMA

On August 23rd, 2003, NASA's Spitzer space telescope (formerly SIRTF) was launched. Among its first results came the source counts at $24\,\mu$m down to $\sim 20\,\mu$Jy which confirmed what ISO deep surveys already saw: a strong excess of faint sources indicating a rapid redshift evolution of IR luminous
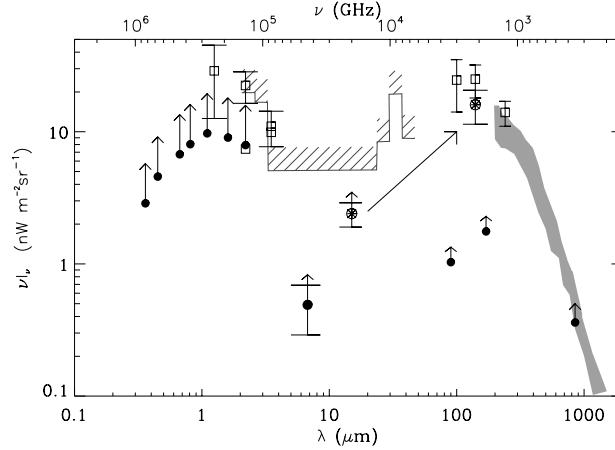
Figure 16. Integrated Galaxy Light (IGL, filled dots) and Extragalactic Background Light (EBL, open squares, grey area) from the UV to sub-millimeter (from Elbaz *et al.* 2002). EBL measurements from COBE: 200-1500 μm EBL from COBE-FIRAS (grey area, Lagache *et al.* 1999), 1.25, 2.2, 3.5, 100, 140 μm EBL from COBE-DIRBE (open squares). IGL in the U,B,V,I,J,H,K bands from Madau & Pozzetti (2000). The upper end of the arrows indicate the revised values suggested by Bernstein et al. (2001, factor two higher). 6.75 μm (ISO-CAM-LW2 filter) IGL from Metcalfe et al. (2003, filled dot with error bar and arrow). Hatched upper limit from Mkn 501 (Stanev & Franceschini 1998). The ISOCAM 15 μm IGL (2.4 $\pm$ 0.5 nW m^{-2} sr^{-1}) is marked with a star surrounded by a circle. The other star surrounded by a circle is the prediction of the contribution of the 15 μm sources to 140 μm (Elbaz *et al.* 2002).

galaxies. When compared to models developed to fit the ISO counts, the faint end of the Spitzer counts are perfectly fitted as shown in the Fig. 17 reproduced from Chary *et al.* (2004). On the high flux density range, around 1 mJy and above, less galaxies are found than predicted by those models (see also Papovich *et al.* 2004). This is partly, if not integrally, due to the fact that even ISOCAM-15 μm number counts were initially overestimated above $S_{15} \sim 1$ mJy as discussed in Sect. 5.1, since the data reduction techniques were not optimized for the surveys with little redundancy over a given sky pixel. Although some refinement of the template SEDs used in the models might be considered (as suggested by Lagache *et al.* 2004), the 24 μm number counts appear to be perfectly consistent with the up-to-date 15 μm counts. Moreover, the high flux density range does not strongly affect the conclusions of the models based on previous 15 μm counts since bright objects do not contribute significantly to the CIRB and to the cosmic density of star formation. Hence these refinements are not strongly affecting the conclusions derived on galaxy formation and evolution based on the ISO deep surveys and summarized in the previous sections (see also Dole *et al.* 2004 for the Spitzer counts in the far IR).
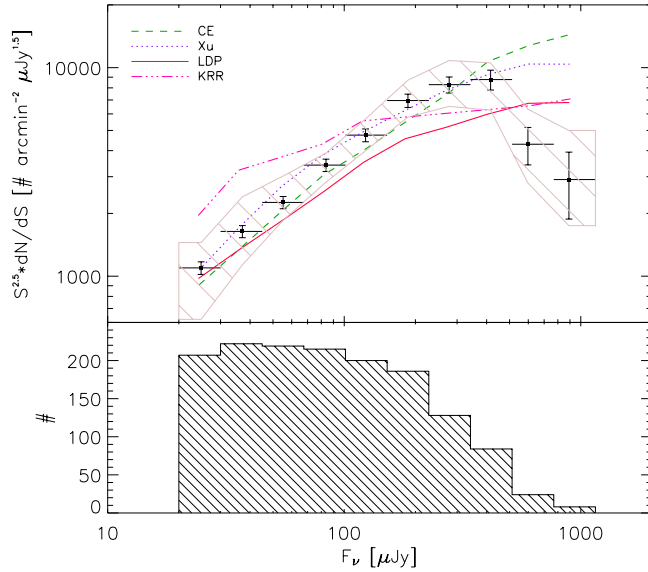
Figure 17. Completeness corrected galaxy counts in the MIPS 24 μm channel from Spitzer observations of the ELAIS-N1 field (from Chary *et al.* 2004). The error bars reflect the Poissonian uncertainty. The horizontal bars represent the minimum and maximum flux density in that bin. The lines show four models for 24 μm counts: King & Rowan-Robinson (2003, KRR), Xu *et al.* (2001, Xu), Chary & Elbaz (2001, CE), Lagache, Dole & Puget (2003, LDP). The symbols are plotted at the average of the flux densities of the detected sources in that bin for the data while the lines are plotted at the counts-weighted flux average for the models. The lower plot in the figure shows the histogram of the actual number of sources detected in each flux bin without any completeness correction.
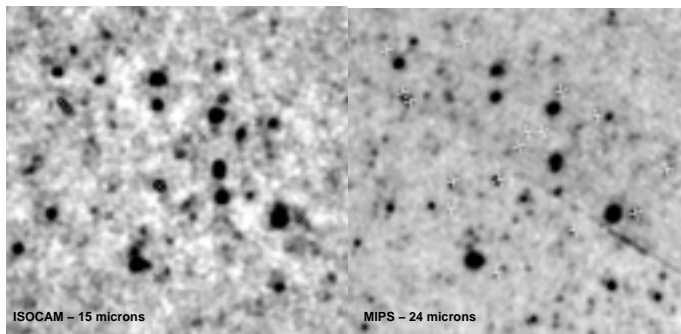

Figure 18. ISOCAM 15 μm image (left) of the Ultra-Deep Survey in the Marano FIRBACK field (depth 140 μJy, 80 % completeness) versus Spitzer MIPS-24 μm image (right; depth 110 μJy, 80 % completeness). The crosses identify 16 galaxies detected at 15 and 24 μm for which VLT-FORS2 spectra were obtained and which SEDs were fitted in Elbaz *et al.* (2004).

Another hint on the consistency of Spitzer MIPS-24 μm surveys with ISOCAM-15 μm is given by the comparison of the images themselves. Galaxies detected at 15 and 24 μm are clearly visible in both images in Fig. 18, although several 24 μm sources do not have a 15 μm counterpart. This results from the combination of the better sensitivity of MIPS, by a factor 2 or slightly more for the deepest surveys (galaxies are detected down to $S_{15} \sim 40$ μJy in the HDFN, see Aussel *et al.* 1999, without lensing magnification), and of the k-correction. For galaxies above $z \sim 1$, the PAH bump centered on the PAH feature at 7.7 μm starts to exit to 15 μm broadband while it remains within the MIPS-24 μm band up to $z \sim 2$. The combination of ISOCAM and MIPS can be used to test whether the library of template SEDs that were used to derive "bolometric" IR luminosities from 8 to 1000 μm for the 15 μm galaxies are correct at least in the mid IR range. One of the most important test is to check whether the 7.7 μm PAH bump is still present at $z \sim 1$ and whether the 24 over 15 μm flux density ratio is consistent with the template SEDs used by the models from which star formation histories were derived. The template SEDs designed by Chary & Elbaz (2001) provide a very good fit to the combination of both mid IR values for a sample of 16 galaxies detected by ISOCAM and MIPS (crosses on the Fig. 18). The L_{IR}(8-1000 μm) derived from either the 15 or 24 μm luminosities or the combination of both to constrain the SED fit present a 1-σ dispersion of only 20 % (Elbaz *et al.* 2004). For galaxies located around $z \sim 1$, the relative 15 and 24 μm luminosities clearly suggest the presence of a bump at 7.7 μm as observed in nearby galaxies and due to PAHs.

Many questions remain unsolved that will be addressed by future missions, staring with Spitzer. Only when a fair sample of redshifts will have been determined for the distant LIRGs will we be able to definitely ascertain the redshift evolution of the IR luminosity function. Already for the brightest part of it, campaigns of redshift measurements have started, on ELAIS fields for the nearby objects, and on the Marano field with VIMOS and the Lockman Hole with DEIMOS for more distant objects. The fields selected for Spitzer legacy and garanteed time surveys were also carefully selected to be covered at all wavelengths and followed spectroscopically, so that this issue should be addressed in the very near future. Due to confusion and sensitivity limits, direct observations in the far IR will not reach the same depth than mid IR ones until the launch of Herschel scheduled for 2007. The direct access to the far IR distant universe with Herschel will certainly bring major information on galaxy formation, together with the James Webb Space Telescope (JWST) up to 30 μm and the Atacama Large Millimeter Array (ALMA), which will bring an improved spatial resolution for the $z \sim 2$ and above universe. Among the questions to be solved, we do not resist to the temptation of listing some of our favorite ones: what is the connection of large-scale structure formation with LIRG phases in galaxies ? Can we probe the formation of distant clusters

by the detection of the epoch when galaxies formed stars in such intense starbursts, producing galactic winds and enriching the intra-cluster medium with metals ? Have we really resolved the bulk of the hard X-ray background, which peaks around 30 keV, and not left unknown some deeply buried AGNs which could make a larger than 20 % fraction of the mid IR light from distant LIRGs ? What is the future of a distant LIRG, is it producing stars in a future bulge or disk ? How uncertain is the interpolation to lower luminosities than those observed done in the models used to derive cosmic star formation history scenarios ? This is of course only an example of a vast series of questions which indicate that the field opened for a large part by ISO has a long life to come.

References

Adelberger, K.L., Steidel, C.C., 2000, ApJ 544, 218

Altieri *et al.* , 1999, A&A 343, L65

Appleton, P.N., Fadda, D.T., Marleau, F.R. *et al.* , 2004, ApJS 154, 147

Aussel, H., Cesarsky, C.J., Elbaz, D., Starck, J.L. 1999, A&A 342, 313

Balland C., Devriendt, J., Silk J., 2003, MNRAS 343, 107

Barger, A.J., Cowie, L.L., Sanders, D.B. *et al.* , 1998, Nature 394, 248

Bernstein, R.A., Freedman, W. L., Madore, B.F., 2002, ApJ 571, 56

Blommaert, J., Siebenmorgen, R., Coulais, A. *et al.* , 2003, 'The ISO Handbook, Volume II: CAM - The ISO Camera', ESA SP–1262

Bruzual, G., Charlot, S., 2003, MNRAS 344, 1000

Butcher, H., Oemler, A., 1984, ApJ 285, 426

Cardiel, N., Elbaz, D., Schiavon, R.P., *et al.* 2003, ApJ 584, 76

Cesarsky, C., Abergel, A., Agnèse, P. *et al.* , 1996, A&A 315, L32

Chapman, S. C., Smail I., Ivison R. *et al.* , 2002, ApJ 573, 66

Chapman, S.C., Blain, A.W., Ivison, R.J., Smail, I. 2003, Nature 422, 695

Chary, R.R., Elbaz, D. 2001, ApJ 556, 562

Chary, R.R., Casertano, S., Dickinson, M.E. *et al.* , 2004, ApJS 154, 80

Ciliegi P., McMahon R. G., Miley G. *et al.* , 1999, MNRAS 302, 222

Clements, D. *et al.* , 1999, A&A 346, 383

Cohen, J.G., Hogg, D.W., Blandford, R. *et al.* , 2000, ApJ 538, 29

Cole, S. *et al.* , 2001, MNRAS 326, 255

Désert F-X., Puget J-L., Clements D., et al., 1999, A&A 342, 363

Devriendt, J.& Guiderdoni, B., 2000, A&A 363, 851

Dickinson, M., Papovich, C., Ferguson, H.C., Budaári, T., 2003, ApJ 587, 25

Dole, H., Gispert, R., Lagache, G. *et al.* , 2000, Springer Lect. Notes in Ph., v548, 54 (astro-ph/0002283)

Dole H., Gispert R., Lagache, G. *et al.* , 2001, A&A 372, 364

Dole, H., 2002, Proceedings of the ESA SP-511 conference "Exploiting the ISO Data Archive - Infrared Astronomy in the Internet Age", C.Gry *et al.* eds. (astro-ph/0211310)

Dole, H., Le Floc'h, E., Perez-Gonzalez, P.G. *et al.* , 2004, ApJS 154, 87

Duc, P.-A., Poggianti, B., Fadda, D. *et al.* , 2002, A&A 382, 60

Duc, P.-A., Fadda, D., Poggianti, B. *et al.* , 2004, Proceedings of the IAU Colloquium 195, "Outskirts of Galaxy Clusters: intense life in the suburbs", Ed. A.Diaferio (astro-ph/0404183)

Efstathiou A., Oliver S., Rowan-Robinson M. *et al.* , 2000, MNRAS, 319, 1169

Elbaz, D., Cesarsky, C.J., Fadda, D. *et al.* , 1999, A&A 351, L37

Elbaz, D., Cesarsky, C.J., Chanial, P. *et al.* , 2002, A&A 384, 848

Elbaz, D., Cesarsky, C.J. 2003, Science 300, 270

Elbaz, D., Moy, E., 2004, Proceedgins of the "Multiwavelength Cosmology" Conference, held on Mykonos Island, Greece, Ed. M. Plionis, Kluwer Academic Publishers, p.173 (astro-ph/0401617)

Elbaz, D., Dole, H., Le F'loch, E., Marcillac, D., 2004, to be submitted

Fadda, D., Elbaz, D., Duc, P.-A., *et al.* 2000, A&A 361, 827

Fadda, D., Flores, H., Hasinger, G. *et al.* , 2002, A&A 383, 838

Fadda, D., Lari, G., Rodighiero, G. *et al.* , 2004, A&A in press (astro-ph/0407649)

Fang, F., Shupe, D., Xu, C., Hacking, P., 1998, ApJ 500, 693

Fixsen, D. J., Dwek, E., Mather, J.C., Bennett, C.L., Shafer, R.A. 1998, ApJ 508, 123

Flores, H., Hammer, F., Thuan, T.X. *et al.* , 1999, ApJ 517, 148

Flores, H., Hammer, F., Elbaz, D., *et al.* , 2004, A&A 415, 885

Franceschini A., Aussel H., Cesarsky C. J., Elbaz D., Fadda D., 2001, A&A 378, 1

Franceschini, A., Berta, S., Rigopoulou, D. *et al.* , 2003, A&A 403, 501

Garrett, M., 2002, A&A 384, L19

Genzel R., & Cesarsky C., 2000, ARAA, 38, 761

Goldader, J.D., Meurer, G., Heckman, T.M. *et al.* , 2002, ApJ 568, 651

Goldschmidt *et al.* , 1997, MNRAS 289, 465

Gonzalez-Solares, E.A., Oliver, S., Gruppioni, C. *et al.* , 2004, MNRAS 352, 44

Gruppioni, C., Pozzi, F., Zamorani, G. *et al.* , 2003, MNRAS 341, L1

Haarsma, D.B., Partridge, R.B., Windhorst, R.A., Richards, E.A., 2000, ApJ 544, 641

Hauser, M.,& Dwek, E., 2001, ARAA, 37, 249

Herbstmeierer U., Abraham P., Lemke D. *et al.* , 1998, A&A 332, 739

Hughes, D. H., Serjeant, S., Dunlop, J., et al. 1998, Nature 394, 241

Juvela M., Mattila K., Lemke D., 2000, A&A 360, 813

Kakazu Y., Sanders D., Jpseph R., et al., 2002, IAU184, astro-ph/0201326

Kawara K., Sato Y., Matsuhara H. *et al.* , 1998, A&A 336, L9

Kawara K., Matsuhara H., Okuda H. *et al.* , 2004, A&A 413, 843

Kessler, M., Steinz, J., Anderegg, M. *et al.* , 1996, A&A 315, L27

Kessler, M.F., Mueller, T.G., Leech, K. *et al.* , 2003, 'The ISO Handbook, Volume I: ISO - Mission & Satellite Overview', ESA SP–1262

King, A. J., & Rowan-Robinson, M., 2003, MNRAS 339, 260

Kim, D.-C., Sanders, D. B., 1998, ApJS 119, 41

Kiss C., Abraham P., Klaas, U. *et al.* , 2001, A&A 379, 1161

Lagache, G., Abergel, A., Boulanger, F. *et al.* , 1999, A&A 344, 322

Lagache G. & Puget J-L., 2000 , A&A 355, 17

Lagache G., Dole H., Puget J-L., 2003, A&A MNRAS 338, 555

Lagache G., Dole H., Puget J-L. *et al.* , 2004, ApJS 154, 112

Lari C., Pozzi F., Gruppioni C. *et al.* , 2001, A&A 325, 1173

Lemke, D., Klaas, U., Abolins, J. *et al.* , 1996, A&A 315, L64

Laureijs, R.J., Klaas, U., Richards, P.J. *et al.* , 2003, 'The ISO Handbook, Volume IV: PHT - The Imaging Photo-Polarimeter', ESA SP–1262

Liang, Y., Hammer, F., Flores, H., Elbaz, D., Cesarsky, C.J., 2004, A&A 423, 867

Lilly, S.J., Le Fevre, O., Hammer, F., Crampton, D., 1996, ApJ 460, L1

Linden-Voernle M.J.D., Norgaard-Nielsen H.U., Jorgensenet H.E. *et al.* , 2000, A&A 359, L51

Madau, P., Ferguson, H.C., Dickinson, M.E., *et al.* 1996, MNRAS 283, 1388

Madau, P., Pozzetti, L. 2000, MNRAS 312, L9

Malkan M., & Stecker F., 2001, ApJ 555, 641

Marcillac, D., Elbaz, D., Charlot, S. *et al.* , 2004, submitted to A&A

Matsuhara H., Kawara K., Sato Y. *et al.* , 2000, A&A 361, 407

Metcalfe, L., Kneib, J.-P., McBreen, B. *et al.* , 2003, A&A 407, 791

Meurer, G.R., Heckman, T.M., Calzetti, D., 1999, ApJ 521, 64

Miville-Deschênes M-A., Lagache G., Puget J-L., 2002, 393, 749

Okumura, K., 1998, ESA ISOCAM PSF Report, Version 1.0, 26 June 1998 (see ISOCAM
    documentation under http://www.iso.vilspa.esa.es)

Oliver S. *et al.* , 1996, MNRAS, 280, 673

Oliver S., Rowan-Robinson, M., Alexander D. *et al.* , 2000, MNRAS, 316, 749

Oliver, S., Mann, R.G., Carballo, R. *et al.* , 2002, MNRAS 332, 536

Papovich, C., Dole, H., Egami, E. *et al.* , 2004, ApJS 154, 70

Patris, J., Dennefeld, M., Lagache, G., Dole, H., 2003, A&A 412, 349

Pearson C., 2001, MNRAS, 325, 1511

Puget, J-L., Abergel, A., Bernard, J-P. *et al.* , 1996, A&A 308, L5

Puget J-L., Lagache G., Clements D. *et al.* , 1999, A&A 345, 29

Puget J-L.,& Lagache G., 2000, IAU204, astro-ph/0101105

Rigopoulou, D., Spoon, H.W.W., Genzel, R. *et al.* , 1999, AJ 118, 2625

Rigopoulou, D., Franceschini, A., Aussel, H. *et al.* , 2000, ApJ 537, L85.

Roche N., & Eales S., 1999, MNRAS, 307, 111

Rodighiero, G., Franceschini, A., 2004, A&A 419, L55

Rodighiero, G., Lari, C., Fadda, D. *et al.* , 2004, A&A in press (astro-ph/0407639)

Rowan-Robinson M., 2001, ApJ 549, 745

Rowan-Robinson, M., Lari, C., Perez-Fournon, I. *et al.* , 2004, MNRAS 351, 1290

Rush, B., Malkan, M.A., Spinoglio, L. 1993, ApJS 89, 1

Sanders, D.B., Mirabel, I.F. 1996, ARA&A 34, 749

Sanders, D., Surace, J.A., Ishida, C.M., 1999, in "Galaxy Interactions at Low and High
    Redshift" IAU Symposium 186, Kyoto, Japan, eds. J.E. Barnes and D.B. Sanders
    (astro-ph/9909114)

Sato, Y., Kawara, K., Cowie, L.L. *et al.* , 2003, A&A 405, 833

Sato, Y., Cowie, L.L., Kawara, K. *et al.* , 2004, AJ 127, 1285

Serjeant S., Oliver S., Rowan-Robinson M. *et al.* , 2000, MNRAS, 316, 768

Serjeant S., Efstathiou A., Oliver S. *et al.* , 2001, MNRAS, 322, 262

Smail, I., Ivison, R.J., Blain, A.W., Kneib, J.-P. 2002, MNRAS 331, 495

Stanev, T., Franceschini, A. 1998, ApJ 494, L159

Starck J.-L., Aussel H., Elbaz D. et al, 1999, A&AS 138, 365

Steidel, C.C., Adelberger, K.L., Giavalisco, M., *et al.* , 1999, ApJ 519, 1

Stickel M., Bogun S., Lemke D. *et al.* , 1998, A&A 336, 116

Stickel M., Lemke D., Klaas U. *et al.* , 2000, A&A 359, 865

Takeuchi T., Ishii T., Hirashita H., et al., 2001, PASJ, 53, 37

Tan J., Silk J., Balland C., 1999, ApJ 522, 579

Taniguchi Y., Cowie, L.L., Sato, Y. *et al.* , 1997, A&A 328, L9

Totani T., & Takeuchi T., 2002, ApJ 570, 470

Tran, Q.D., Lutz, D., Genzel, R. *et al.* , 2001, ApJ 552, 527

Wang Y., 2002, A&A 383, 755

Wirth, G.D., Willmer, C.N.A., Amico, P. *et al.* , 2004, AJ 127, 3121

Xu, C., Hacking, P., Fang, F. *et al.* , 1998, ApJ 508, 576

Xu, C., Lonsdale, C., Shupe, D. *et al.* , 2001, ApJ 562, 179

Xu, C. K., Lonsdale, C. J., Shupe, D. L. *et al.* , 2003, ApJ 587, 90